[DOI]10.12016/j.issn.2096-1456.202550195

·基础研究·

白藜芦醇碳化聚合物点对炎症状态下的巨噬细胞极化及人牙周膜干细胞成骨分化的影响

李诺[1]，　王玉龙[2]，　柳庆[3]，　苗雷英[1]

1.南京大学医学院附属口腔医院，南京市口腔医院牙体牙髓病科，南京大学口腔医学研究所，江苏 南京（210008）；　2.牡丹江市第二人民医院口腔科，黑龙江 牡丹江（157000）；　3.南京大学医学院附属口腔医院，南京市口腔医院牙周科，南京大学口腔医学研究所，江苏 南京（210008）

【摘要】　目的　探讨白藜芦醇碳化聚合物点（resveratrol-derived carbonized polymer dots，RSV-CPDs）对炎症状态下的巨噬细胞极化与人牙周膜干细胞（human periodontal ligament stem cells，hPDLSCs）成骨分化的作用及其机制，为RSV-CPDs治疗牙周炎提供实验依据。**方法**　将白藜芦醇（resveratrol，RSV）在催化剂氨水存在的条件下通过高温热解法制备成RSV-CPDs并且通过透射电镜（transmission electron microscope，TEM）、傅里叶红外光谱（Fourier transform infrared spectrometer，FTIR）、X射线衍射（X-ray diffraction，XRD）以及X射线光电子能谱（X-ray photoelectron spectroscopy，XPS）对RSV-CPDs进行表征验证；使用CCK8检测RSV-CPDs的细胞毒性。通过流式细胞术检测RSV-CPDs在牙龈卟啉单胞菌来源的脂多糖（*Porphyromonas gingivalis*-lipopolysaccharide，*P.g*-LPS）刺激条件下对巨噬细胞的凋亡及细胞极化的影响：①细胞凋亡实验分组：将巨噬细胞（RAW264.7）分为对照组（不做任何处理）、*P.g*-LPS组[*P.g*-LPS（2 μg/mL）处理细胞24 h]、RSV组[*P.g*-LPS（2 μg/mL）+RSV（10 μg/mL）处理细胞24 h]以及RSV-CPDs组[*P.g*-LPS（2 μg/mL）+ RSV-CPDs（50 μg/mL）处理细胞24 h]，；②细胞极化实验分组：将巨噬细胞（RAW264.7）分为4组，分别为对照组（不做任何处理）、*P.g*-LPS+IFN-γ组[*P.g*-LPS（200 ng/mL）+IFN-γ（20 ng/mL）处理细胞24 h]、RSV组[*P.g*-LPS（200 ng/mL）+IFN-γ（20 ng/mL）+RSV（10 μg/ml）处理细胞24 h]、RSV-CPDs组[*P.g*-LPS（200 ng/mL）+IFN-γ（20 ng/mL）+ RSV-CPDs（50 μg/mL）处理细胞24 h]。收集上述细胞极化实验中各组巨噬细胞上清液并与成骨诱导培养基1∶1混合，分别用于培养hPDLSCs，将hPDLSCs对应分组为对照组、*P.g*-LPS+IFN-γ组、RSV组以及RSV-CPDs组，采用碱性磷酸酶染色（alkaline phosphatase，ALP）、茜素红染色（alizarin red staining，ARS）检测hPDLSCs成骨趋势；实时定量PCR（real-time quantitative PCR，RT-qPCR）检测成骨相关基因表达的变化；Western blot检测hPDLSCs的成骨相关蛋白的表达结果。最后采用转录组学测试探究RSV-CPDs对炎症刺激下的巨噬细胞（THP-1）表型影响的机制。**结果**　TEM结果显示RSV-CPDs呈现均一的球形结构；FTIR结果显示，RSV-CPDs产生新的O-C=O峰；XRD结果证实新合成的RSV-CPDs呈现无定形结构；XPS结果显示RSV-CPDs形成了亲水基团羧基；CCK-8结果显示RSV在浓度超过10 μg/mL时便对RAW264.7存在一定的毒性（*P*=0.011），而RSV-CPDs在浓度达到50 μg/mL时对细胞依旧具有良好的生物安全性（*P*>0.05），因此后续试验浓度RSV为10 μg/mL，RSV-CPDs为50 μg/mL。流式细胞术结果显示：RSV-CPDs具有抑制炎性刺激状态下巨噬细胞凋亡的效果（*P*=0.008），且抑制效果优于其前体RSV（*P*=0.009）。RSV组以及RSV-CPDs组$CD86^+$细胞相较于*P.g*-LPS+IFN-γ组有不同程度的降低（*P*<0.001，*P*=0.004），而$CD206^+$细胞则存在不同程度的提升（*P*=0.006，*P*=0.008），并且RSV-CPDs组$CD206^+$细胞比例高于RSV组（*P*=0.010）。与*P.g*-LPS+IFN-γ组对比，RSV-CPDs处理过的巨噬细胞上清液显著提升了hPDLSCs的ALP表达（*P*=0.005）、ARS水平（*P*=0.006），成骨相关基因RUNX-2、OCN以及COL-1的mRNA表达显著上升（*P*<0.05），以及RUNX-2蛋白水平也显著上升（*P*=0.001）。转录组学结果显示：与*P.g*-LPS+IFN-γ组对比，RSV-

【收稿日期】2025-05-13；【修回日期】2025-07-10

【基金项目】江苏省科技计划专项资金（基础研究计划自然科学基金）（BK20221177）；2024年江苏省干部保健科研（BJ24041）；南京市卫生科技发展专项资金重点项目（ZKX24056）；南京市口腔医院高水平医院建设科研项目（0024C006）

【作者简介】李诺，博士研究生，Email：nuoli97@163.com

【通信作者】苗雷英，主任医师，教授，博士，Email：miaoleiying80@163.com

CPDs组的核因子κB(nuclear factor kappa-B,NF-κB)信号通路以及肿瘤坏死因子(tumor necrosis factor,TNF)信号通路均呈现下调趋势。**结论**　RSV-CPDs可抑制炎症状态下的巨噬细胞凋亡及使其向M2型极化,促进hPDLSCs成骨分化,其机制可能与抑制NF-κB、TNF信号通路有关。

【关键词】　巨噬细胞极化；　牙龈卟啉单胞菌；　白藜芦醇；　碳化聚合物点；　脂多糖；　炎症；　人牙周膜干细胞；　成骨分化

【中图分类号】　R78　**【文献标志码】**　A　**【文章编号】**　2096-1456(2025)10-0827-14

【引用著录格式】　李诺,王玉龙,柳庆,等.白藜芦醇碳化聚合物点对炎症状态下的巨噬细胞极化及人牙周膜干细胞成骨分化的影响[J].口腔疾病防治,2025,33(10):827-840. doi:10.12016/j.issn.2096-1456.202550195.

微信公众号

Effects of resveratrol-derived carbonized polymer dots on macrophage polarization and osteogenic differentiation of human periodontal ligament stem cells under inflammatory conditions

LI Nuo[1], WANG Yulong[2], LIU Qing[3], MIAO Leiying[1].　1. Department of Cariology and Endodontics, Nanjing Stomatological Hospital, Affiliated Hospital of Medical School, Nanjing University, Research Institute of Stomatology, Nanjing 210008, China;　2. Department of Stomatology, The Second People's Hospital of Mudanjiang, Mudanjiang 157000, China;　3. Department of Periodontology, Nanjing Stomatological Hospital, Affiliated Hospital of Medical School, Research Institute of Stomatology, Nanjing University, Nanjing 210008, China

Corresponding author: MIAO Leiying, Email: miaoleiying80@163.com

【Abstract】　**Objective**　To investigate the effect and mechanism of resveratrol-derived carbonized polymer dots (RSV-CPDs) on macrophage polarization and osteogenic differentiation of human periodontal ligament stem cells (hPDLSCs) under inflammatory conditions, and to provide an experimental basis for the treatment of periodontitis with RSV-CPDs. **Methods**　RSV-CPDs were prepared by high-temperature pyrolysis of resveratrol (RSV) in the presence of ammonia as a catalyst, and RSV-CPDs were characterized by transmission electron microscope (TEM), Fourier transform infrared spectrometer (FTIR), X-ray diffraction (XRD), and X-ray photoelectron spectroscopy (XPS). CCK8 was used to detect the cytotoxicity of RSV-CPDs. The effects of RSV-CPDs on the apoptosis and cell polarization of macrophages stimulated by *Porphyromonas gingivalis*-lipopolysaccharide (*P.g*-LPS) were detected by flow cytometry: ① For the apoptosis detection experiment, the macrophages (RAW264.7) were divided into the control group (no treatment), *P.g*-LPS group [treated with *P.g*-LPS (2 μg/mL) for 24 h], RSV group [treated with *P.g*-LPS (2 μg/mL) + RSV (10 μg/mL) for 24 h], and RSV-CPDs group [treated with *P.g*-LPS (2 μg/mL) + RSV-CPDs (50 μg/mL) for 24 h]. ② For the cell polarization experiment, the macrophages (RAW264.7) were divided into four groups. They were the control group (no treatment), *P.g*-LPS + IFN-γ group [*P.g*-LPS (200 ng/mL) + IFN-γ (20 ng/mL) treated cells for 24 h], RSV group [*P.g*-LPS (200 ng/mL) + IFN-γ (20 ng/mL) + RSV (10 μg / mL) treated cells for 24 h], RSV-CPDs group [*P.g*-LPS (200 ng / mL) + IFN-γ (20 ng / mL) + RSV-CPD (50 μg / mL) treated cells for 24 h]. The supernatant of macrophages in the above four groups of cell polarization experiments was collected and mixed with osteogenic induction medium at a 1:1 ratio to culture hPDLSCs. The hPDLSCs were divided into the control group, *P.g*-LPS + IFN-γ group, RSV group, and RSV-CPDs group. The osteogenic trend of hPDLSCs was detected by alkaline phosphatase (ALP) staining and alizarin red staining (ARS). Real-time quantitative PCR (RT-qPCR) was used to detect the expression of osteogenesis-related genes. Western blot was used to detect the expression of osteogenesis-related proteins in hPDLSCs. Finally, transcriptome tests were used to explore the mechanism of the effect of RSV-CPDs on the phenotype of macrophages (THP-1) stimulated by inflammation. **Results**　TEM results showed that RSV-CPDs exhibited a uniform spherical structure. FTIR results showed the O-C=O peak of RSV-CPDs. XRD results confirmed that the newly synthesized RSV-CPDs exhibited an amorphous structure. XPS results showed that RSV-CPDs formed a hydrophilic carboxyl group. CCK-8 results showed that RSV had specific toxicity to RAW264.7 when the concentration exceeded 10 μg/mL (P = 0.011), while RSV-CPDs still had good biosafety to cells when the concentration reached 50 μg/mL (P > 0.05). Therefore, the concentration of RSV was 10 μg/mL and RSV-CPDs was 50 μg/mL. The results of flow cytometry showed that RSV-CPDs inhibited the apoptosis of macrophages under inflammatory stimulation (P = 0.008), and the inhibitory effect was better than that of its precursor RSV (P = 0.009). Compared with the *P.g*-LPS + IFN-γ group, $CD86^+$ cells in the RSV group and RSV-CPDs group decreased by varying degrees (P < 0.001, P = 0.004), while $CD206^+$ cells increased by varying degrees (P = 0.006, P = 0.008), and the proportion of $CD206^+$ cells in the RSV-CPDs group was higher than that in the RSV group (P = 0.010). Compared with the *P.g*-LPS + IFN-γ group, the supernatant of macrophages treated

with RSV-CPDs significantly increased the ALP expression (P = 0.005) and ARS level (P = 0.006) of hPDLSCs. The mRNA expression of osteogenic-related genes RUNX-2, OCN, and COL-1 significantly increased (P < 0.05), and the level of RUNX-2 protein also significantly increased (P = 0.001). Transcriptome results showed that compared with the *P.g*-LPS + IFN-γ group, the nuclear factor kappa-B (NF-κB) signaling pathway and tumor necrosis factor (TNF) signaling pathway in the RSV-CPDs group showed downward trends. **Conclusion**　RSV-CPDs can inhibit the apoptosis of macrophages in the inflammatory state, promote M2 polarization, and bolster the osteogenic differentiation of hPDLSCs. The mechanism involved may be related to the inhibition of NF-κB and TNF signaling pathways.

【Key words】 macrophage polarization; *Porphyromonas gingivalis*; resveratrol; carbonized polymer dots; lipopolysaccharide; inflammation; human periodontal ligament stem cells; osteogenic differentiation
J Prev Treat Stomatol Dis, 2025, 33(10): 827-840.
【Competing interests】 The authors declare no competing interests.
This study was supported by the grants from Natural Science Foundation of the Basic Research Program, Jiangsu Provincial Science and Technology Department (No. BK20221177); 2024 Jiangsu Province Scientific Research Program for Cadre Healthcare (No. BJ24041); Key Project of Nanjing Medical Science and Technology Development Program (No. ZKX24056); High-Level Hospital Construction Project of Nanjing Stomatological Hospital, Affiliated Hospital of Medical School, Institute of Stomatology, Nanjing University (No. 0024C006).

慢性牙周炎是一种常见的口腔疾患，全球约20%～50%的人受其影响[1]。牙齿出血、口腔异味、牙齿松动甚至脱落是慢性牙周炎的主要临床表现[2]。此外，患有严重牙周炎的人更容易患心血管疾病、糖尿病和阿尔茨海默病等，这些疾病都可能对全身健康产生影响[3]。在牙周炎病损区，炎性免疫细胞过度活跃，产生的炎症因子诱发破骨细胞过度活跃，最终导致牙槽骨的吸收[4]。巨噬细胞在炎症刺激情况下会极化为M1表型，属“经典”型巨噬细胞，主要分泌促炎因子。而在炎症缓解过程中会极化为M2表型，属于“替换”型巨噬细胞，发挥抗炎作用[5]。既往研究证实牙周组织内的巨噬细胞在极化为M2表型后，所分泌的细胞因子通过巨噬细胞与干细胞间的“cross-talk”作用促进hPDLSCs分化为成骨细胞[6]。因此，选用合适的策略抑制牙周病损区过度的炎症反应，促进牙槽骨再生对于牙周炎的治疗是很有意义的[7-8]。

白藜芦醇（resveratrol，RSV）是一种多酚化合物，具有良好的抗菌、抗炎、抗氧化以及抗肿瘤的效果[9]。这些优势为RSV应用于牙周炎的治疗提供了强有力的支持。然而，RSV水溶性较差，并存在一定程度的细胞毒性，这些缺陷限制了其进一步的生物应用[10]。因此，选择合适的策略在提升RSV水溶性、生物安全性的同时，保留RSV的优势成为重中之重。碳化聚合物点（carbonized polymer dots，CPDs）是一类新兴的碳基纳米颗粒，通常是通过水热或溶剂热方法从多官能度有机小分子或聚合物前体中制备而得。其表面的聚合物壳层有丰富的官能团，赋予CPDs良好的水分散性[11-12]。共价碳骨架结构也增强了CPDs的稳定性，并具有更低的毒性、更低的成本和优异的生物相容性，这些特点对生物相关领域的实际应用至关重要[13-14]。本课题组前期关于RSV抗炎、抗氧化以及促进骨再生等效果已经进行过充分的验证[15]，但是将疏水的RSV制备成水分散性良好的碳化聚合物点之前并未被其他课题组报道，其成骨效果亦未得到验证。基于以上，本课题组通过对RSV施加一定的温度和压力，诱导形成白藜芦醇碳化聚合物点（resveratrol-derived carbonized polymer dots，RSV-CPDs）。将RSV-CPDs与炎症状态下的巨噬细胞共培养并观察其对巨噬细胞表型的影响以及机制探究，验证了RSV-CPDs刺激后的巨噬细胞上清液对人牙周膜干细胞（human Periodontal Ligament Stem Cells，hPDLSCs）成骨分化的促进效果，为RSV-CPDs治疗牙周炎提供实验依据。

1　材料和方法

1.1　主要试剂与仪器

DMEM-高糖（11965118，Gibco，美国），胎牛血清（FSS500，依科赛，中国），青霉素/链霉素（SV30010，Hyclone，美国），PBS（G4202，Servicebio，中国），CCK-8试剂盒（CK04，同仁，日本），RSV（R0071，TCI，日本），微孔滤菌过滤器（SLGV004SL，Sigma-Aldrich，美国），透析袋（02048716，泰坦科技探索平台，中国），小鼠巨噬细胞系RAW264.7细胞、人源性巨噬细胞THP-1（上海细胞库，中国），

hPDLSCs(CP-H234,武汉普诺赛生命科技有限公司,中国),RT-qPCR 试剂盒(RC112,R323,Q711,诺维赞,中国),Annexin V-PI 试剂盒(BB-4101,Bestbio,中国),PE-CD206(大鼠抗小鼠)、APC-CD86(大鼠抗小鼠)、CD16/CD32(人IgG4抗小鼠)(163403,159215,141705,Biolegend,美国),碱性磷酸酶染色(alkaline phosphatase,ALP)检测试剂盒(C3206,P0321S碧云天,中国),茜素红染色(alizarin red staining,ARS)试剂盒(G1452,Solarbio,中国),氯化十六烷基吡啶一水合物(6004-24-6,Sigma-Aldrich,美国),重组anti-RUNX-2抗体(兔单克隆抗体,Abcam,ab236639,美国),β-actin抗体(兔多克隆抗体,Proteintech,20536-1-AP,美国),二抗山羊抗兔抗体(Ab2337913,Jackson,美国),SurePAGE™ 预制胶,电泳缓冲液(M42012C,M00138,金斯瑞,中国),TBST(C006161,生工,中国),PVDF膜(IPVH00010,Millipor,美国),牙龈卟啉单胞菌来源的LPS(*Porphyromonas gingivalis*-lipopolysaccharide,*P.g*-LPS,InvivoGen,美国),干扰素-γ(IFN-γ,Z02916-100,金斯瑞,中国)。

聚四氟乙烯内衬不锈钢高压釜(Rs13602,Shilpa Enterprises,美国),透射电子显微镜(JEM-F200,JEOL,日本),红外光谱仪(iS20,Thermo Fisher Scientific Nicolet,美国),拉曼光谱仪(LabRAM HR Evolution,Horiba,日本),X线衍射仪(D8 Advance,Bruker,美国),酶标仪(SpectraMAXM3,Thermo Scientific,美国),X射线光电子能谱仪(ESCALAB 250Xi,ESCALAB 250Xi,美国),流式细胞仪(FACS Calibur,BD,美国),倒置荧光显微镜(NikonTi2,Nikon 日本),Nanodrop核酸检测仪(One,Thermo Scientific,美国),RNA逆转录分析仪(C1000 Touch,Bio-Rad,美国),RT-qPCR分析仪(ViiA V7Dx,Thermo,美国),Trizol试剂(15596026,Invitrogen,美国),QuantiCyto®小鼠转化生长因子-β1(transforming growth factor-β1,TGF-β1)酶联免疫吸附(enzyme-linked immunosorbent assay,ELISA)试剂盒(EMC107b.48,欣博盛,中国)。

1.2　RSV-CPDs的制备、表征验证及细胞毒性检测

1.2.1　RSV-CPDs的制备　将340 mg RSV和6 mL氨水(v/v:25%~28%)通过超声处理溶解在超纯水(54 mL)中15 min,得到RSV溶液。随后,将每15 mL RSV溶液加入25 mL内衬特氟纶的不锈钢高压釜中,在200 ℃的烘箱中加热4 h。反应器自然冷却至室温后,将反应溶液通过0.22 μm微孔膜过滤以去除大块沉淀物,得到透明的棕色溶液。溶液最初在截留分子量为1 kDa的透析袋中用超纯水透析,以去除残留的小分子物质和氨,随后用稀释的氨溶液(pH值≈9)透析,以完全去除残留的大分子物质。最后,再次用超纯水透析溶液以去除残留的氨,可以获得纯化的RSV-CPDs。取出固定体积的溶液并冷冻干燥,以测定RSV-CPDs的浓度。

1.2.2　RSV及RSV-CPDs的表征验证　TEM成像在JEOL JEM-F200透射电子显微镜上完成。红外光谱测量是在傅里叶红外光谱(Fourier transform infrared spectrometer,FTIR)光谱仪上进行,光谱分辨率为4 cm^{-1}。X射线衍射(X-ray diffraction,XRD)测量是通过配备CuKα辐射(λ=0.15 406 nm)的SmartLab SE射线衍射仪进行测试。X射线光电子能谱(X-ray photoelectron spectroscopy,XPS)是通过赛默飞世尔科技ESCALAB 250Xi XPS系统进行测试,使用XPS PEAK41软件减去Shirley背景后,使用高斯-洛伦兹分量轮廓拟合高分辨率XPS光谱。

1.2.3　RSV及RSV-CPDs的细胞毒性测试　小鼠巨噬细胞(RAW264.7)细胞在含有10%(v/v)胎牛血清和1%青霉素-链霉素(P/S)的Dulbecco's Modified Eagle培养基中培养,温度为37 ℃、二氧化碳含量5%、湿度100%,以每孔5×10^3细胞的密度接种在96孔板中,并使其自然贴壁24 h。待细胞贴壁后,分别用不同浓度的RSV-CPDs(0、5、10、20、50 μg/mL)、不同浓度的RSV(0、2.5、5、10、20 μg/mL)处理细胞24 h,使用10%(v/v)CCK8培养基孵育细胞2 h,并用酶标仪在450 nm吸光度处读数。以RSV、RSV-CPDs浓度为0 μg/mL时的吸光度值换算成平均存活率为100%,并计算其他浓度下的细胞存活率(%)。

1.3　流式细胞术检测RSV-CPDs对巨噬细胞的极化与凋亡的影响

1.3.1　细胞凋亡　①实验分组:待巨噬细胞贴壁后,将细胞随机分为对照组(不做任何处理),仅*P.g*-LPS(2 μg/mL)处理细胞24 h作为*P.g*-LPS组,*P.g*-LPS(2 μg/mL)+RSV(10 μg/mL)处理细胞24 h作为RSV组,*P.g*-LPS(2 μg/mL)+ RSV-CPDs(50 μg/mL)处理细胞24 h作为RSV-CPDs组。②实验操作:24 h后去除培养基,PBS清洗残留培养基后加入Annexin V—FITC和PI染液在4 ℃条件下孵育细胞30 min,最后用PBS洗涤细胞以清除未进入细胞的荧光标记染料。使用流式细胞仪进行分析,FlowJo v10软件进行数据处理。

1.3.2　细胞极化　①实验分组：待巨噬细胞贴壁后，将细胞随机分为对照组（不做任何处理），仅*P.g*-LPS（200 ng/mL）+IFN-γ（20 ng/mL）处理细胞24 h作为*P.g*-LPS+IFN-γ组，*P.g*-LPS（200 ng/mL）+IFN-γ（20 ng/mL）+RSV（10 μg/mL）处理细胞24h作为RSV组，*P.g*-LPS（200 ng/mL）+IFN-γ（20 ng/mL）+RSV-CPDs（50 μg/mL）处理细胞24h作为RSV-CPDs组。②实验操作：24 h后收集RAW264.7细胞并用PBS洗涤3次。然后，首先在4 ℃下用CD16/CD32抗体孵育15 min，随后加入APC-CD86和PE-CD206并孵育30 min，最后用PBS洗涤细胞以清除未进入细胞的荧光标记染料。

1.4　ELISA检测RSV-CPDs处理巨噬细胞后上清液中的TGF-β1水平

巨噬细胞分组与方法1.3.2的一致，分别收集4组（对照组、*P.g*-LPS+IFN-γ组、RSV组与RSV-CPDs组）的RAW264.7上清液。依据ELISA试剂盒生产厂家的说明书进行后续操作：首先利用标准品确定浓度和吸光度的换算公式，然后在涂有TGF-β1抗体的空板内依次加入对照组、*P.g*-LPS+IFN-γ组、RSV组与RSV-CPDs组的上清液孵育90 min。洗去上清液后依次加入生物素化的抗小鼠TGF-β1抗体和辣根过氧化物酶标记的亲和素。最后加入显色底物处理15 min后再加入反应终止液，酶标仪于吸光度450 nm处记录读数。

1.5　hPDLSCs的培养及分组

hPDLSCs用完全培养基DMEM（含有10%（v/v）胎牛血清和1%青霉素-链霉素P/s）并培养在37 ℃，5%CO_2的条件下。细胞融合度超过80%后进行传代，P3～P6代细胞用于后续实验[15]。

收集不同组处理后（同方法1.3.2）的巨噬细胞上清液，将hPDLSCs分为4组，为空白对照组、*P.g*-LPS+IFN-γ组、RSV组与RSV-CPDs组，分别使用对应组别的巨噬细胞上清液与成骨诱导培养基1∶1混合培养[16]，以1×10^4的密度接种在6孔板中，直至细胞黏附、融合度超过90%，每3 d换一次液[17]。

1.6　ALP、ARS实验检测hPDLSCs成骨能力

1.6.1　ALP定量实验　与hPDLSCs培养7 d后，除去细胞上清液，hPDLSCs用4%（v/v）多聚甲醛固定，按照试剂盒说明步骤使ALP显色试剂盒进行染色。染色结果使用白光扫描仪观察样品。ALP定量实验：依据ALP检测试剂盒的说明进行测试。

1.6.2　ARS　与hPDLSCs培养14 d后，除去细胞上清液，hPDLSCs在室温下用70%（v/v）乙醇溶液固定细胞30 min，然后进行茜素红染色。每个样品用2%（w/v）的茜素红S染色30 min。最后使用倒置荧光显微镜和扫描仪观察样品，并进行染料提取定量。将染料在450 μL 10%（w/v）氯化十六烷基吡啶一水合物中提取15 min。将溶液等分并转移到96孔板（每孔150 μL）中，使用微孔板读数器测量波长562 nm处的吸光度。

1.7　RT-qPCR检测hPDLSCs成骨相关基因的mRNA表达

使用RNAprep纯细胞试剂盒提取总RNA，nanodrop测定样本的RNA含量。随后使用PrimeScript RT试剂盒通过逆转录制备cDNA。通过实时PCR仪分析成骨相关的因子的基因表达（引物列见表1）。比较$2^{-\Delta\Delta}$Ct方法用于量化不同mRNA表达的相对水平。所有样本选择GAPDH作为内参，检测骨生成转录因子2（runt-related transcription factor 2，RUNX-2），I型胶原蛋白（collagen type Ⅰ，COL-1）以及骨钙素（osteocalcin，OCN）的水平。

1.8　Western blot检测hPDLSCs成骨相关蛋白水平

将hPDLSCs铺至6孔板中，待细胞融合度超90%后，加入对照组的RAW264.7上清液并与成骨诱导培养基1∶1混合作为对照组；加入*P.g*-LPS+IFN-γ组的RAW264.7上清液并与成骨诱导培养基1∶1混合作为*P.g*-LPS+IFN-γ组；加入RSV组的RAW264.7上清液并与成骨诱导培养基1∶1混合作为RSV组；加入RSV-CPDs组的RAW264.7上清液

表1　RT-qPCR引物序列

Table 1　Primer sequences in RT-qPCR

Genes	Forward primers（5′-3′）	Reverse primers（5′-3′）
RUNX-2	GGAGTGGACGAGGCAAGAGTTT	AGCTTCTGTCTGTGCCTTCTGG
COL-1	AGAACAGCGTGGCCT	TCCGGTGTGACTCGT
OCN	GGCAGCGAGGTAGTGAAGAG	GATGTGGTCAGCCAACTCGT
GAPDH	CGCTCTCTGCTCCTCCTGTT	CCATGGTGTCTGAGCGATGT

RUNX-2: Runt-related transcription factor 2; COL-1: collagen type I; OCN: osteocalcin; GAPDH: glyceraldehyde-3-phosphate dehydrogenase

并与成骨诱导培养基1∶1混合作为RSV-CPDs组。培养7天后，去除原培养基，PBS冲洗3次，加入RIPA裂解液和磷酸酶抑制剂提取细胞总蛋白。测定蛋白浓度后，加入1×SDS上样液并在95 ℃情况下充分变性。电泳凝胶内加入等量（30 μg）蛋白，电泳结束后转至PVDF膜并用5%脱脂奶粉封闭1 h。将RUNX-2与内参β-actin稀释1 000倍后均匀覆盖在PVDF膜上。孵育2 h后洗膜，并以1∶500的比例稀释和孵育二抗山羊抗兔抗体1 h，最后显影并曝光观察蛋白表达情况。

1.9　转录组学分析RSV-CPDs对炎症状态下的巨噬细胞极化作用的机制

选用*P.g*-LPS（200 ng/mL）+IFN-γ（20 ng/mL）刺激人源巨噬细胞（THP-1）24 h，作为*P.g*-LPS+IFN-γ组。加入*P.g*-LPS（200 ng/mL）+IFN-γ（20 ng/mL）的同时再加入50 μg/mL的RSV-CPDs并与THP-1共培养24 h作为RSV-CPDs组。24 h后用PBS洗涤细胞3次，使用Trizol试剂提取总RNA。使用Thermo Scientific分光光度计测量RNA纯度和浓度，并用生物分析仪评估其完整性。随后，根据标准方案，使用VAHTS Universal V6 RNA-seq文库制备试剂盒制备RNA-seq库。Majorbio公司（上海，中国）执行了转录组测序，并提供了后续分析支持。

1.10　统计学分析

采用Prism 9.3.1软件进行作图和统计学分析，正态分布的计量资料以平均值±标准差表示。运用单因素方差分析（one-way ANOVA）对各指标进行比较。$P<0.05$认为差异具有统计学意义。

2　结　果

2.1　RSV-CPDs的表征验证及细胞毒性检测

TEM结果显示高温热解法制备的RSV碳化聚合物点（RSV-CPDs）分散良好并呈现均一的球形结构（图1a），平均直径小于3 nm（图1b）。FTIR结果显示，与RSV的结果相比（图1c），RSV-CPDs在大约1 700 cm^{-1}处形成了新的O-C=O峰（图1d）。XRD结果证实新合成的RSV-CPDs呈现无定形结构（图1e），这与其前体RSV呈现的晶体结构（图1f）差异较大。XPS结果显示，与RSV相比，RSV-CPDs的XPS碳和氧的精细谱分别在结合能288.7 eV、532.3 eV处新形成了羧基（图1g&1h）。上述结果证实了RSV-CPDs的成功合成。

CCK-8实验结果显示，加入50 μg/mL RSV-CPDs共培养的巨噬细胞（RAW264.7）与对照组（0 μg/mL RSV-CPDs）相比，细胞活力无显著性差异（$P>0.05$）（图1i）；加入RSV浓度为10 μg/mL时细胞活力与对照组（0 μg/mL RSV）相比无显著差异（$P>0.05$），而当RSV浓度为20 μg/mL时，与对照组（0 μg/mL RSV）相比，细胞活力显著下降（$P=0.017$）（图1j）。因此，本研究的RSV实验浓度设置为10 μg/mL，RSV-CPDs实验浓度为50 μg/mL。

2.2　RSV-CPDs抑制LPS诱导下的巨噬细胞凋亡

流式细胞术检测细胞凋亡的结果显示（图2），*P.g*-LPS刺激巨噬细胞RAW264.7细胞24 h后，与空白对照组相比，RAW264.7早期凋亡（Q3）比例明显提升（$P=0.015$），RSV组和RSV-CPDs组的RAW264.7早期凋亡（Q3）的比例与*P.g*-LPS组比较，均显著下降（RSV组 *vs.* *P.g*-LPS组：$P=0.048$；RSV-CPDs组 *vs.* *P.g*-LPS组：$P=0.008$），而其中RSV-CPDs组细胞凋亡比例下降作用优于RSV组（$P=0.009$）。

2.3　RSV-CPDs促进炎症状态下巨噬细胞M2型极化

流式细胞术检测细胞极化结果显示（图3），*P.g*-LPS+IFN-γ刺激后的巨噬细胞RAW264.7的M1表型标志物（$CD86^+$）（Q1）相比对照组显著提升（$P<0.001$），而加入RSV和RSV-CPDs后M1表型标志物（$CD86^+$）（Q1）相较于*P.g*-LPS+IFN-γ组有着不同程度的下降（RSV组 *vs.* *P.g*-LPS+IFN-γ组：$P<0.001$；RSV-CPDs组 *vs.* *P.g*-LPS+IFN-γ组：$P=0.004$）。此外，RSV与RSV-CPDs处理的RAW264.7的M2表型标志物（$CD206^+$）（Q3）相较于*P.g*-LPS+IFN-γ亦有显著提升（RSV组 *vs.* *P.g*-LPS+IFN-γ组：$P=0.006$；RSV-CPDs组 *vs.* *P.g*-LPS+IFN-γ组：$P=0.008$），其中RSV-CPDs组提升效果优于RSV组（$P=0.010$）（图3a～3c）。ELISA检测以上各组巨噬细胞上清液的TGF-β1含量，结果显示RSV-CPDs组巨噬细胞上清液内所含有的TGF-β1（M2型巨噬细胞分泌的因子）显著高于对照组和*P.g*-LPS + IFN-γ组（RSV-CPDs组 *vs* 对照组：$P<0.01$；RSV-CPDs组 *vs* *P.g*-LPS + IFN-γ组：$P<0.05$）（图3d）。

2.4　RSV-CPDs诱导的M2表型极化巨噬细胞的上清液可促进hPDLSCs成骨分化

首先对上清液诱导7 d后的hPDLSCs进行ALP染色。结果显示，*P.g*-LPS+IFN-γ组刺激后的巨噬细胞上清液和对照组巨噬细胞上清液诱导的hPDLSCs的ALP颜色较RSV-CPDs组诱导后更弱。同时，RSV-CPDs上清液诱导的hPDLSCs生成的ALP

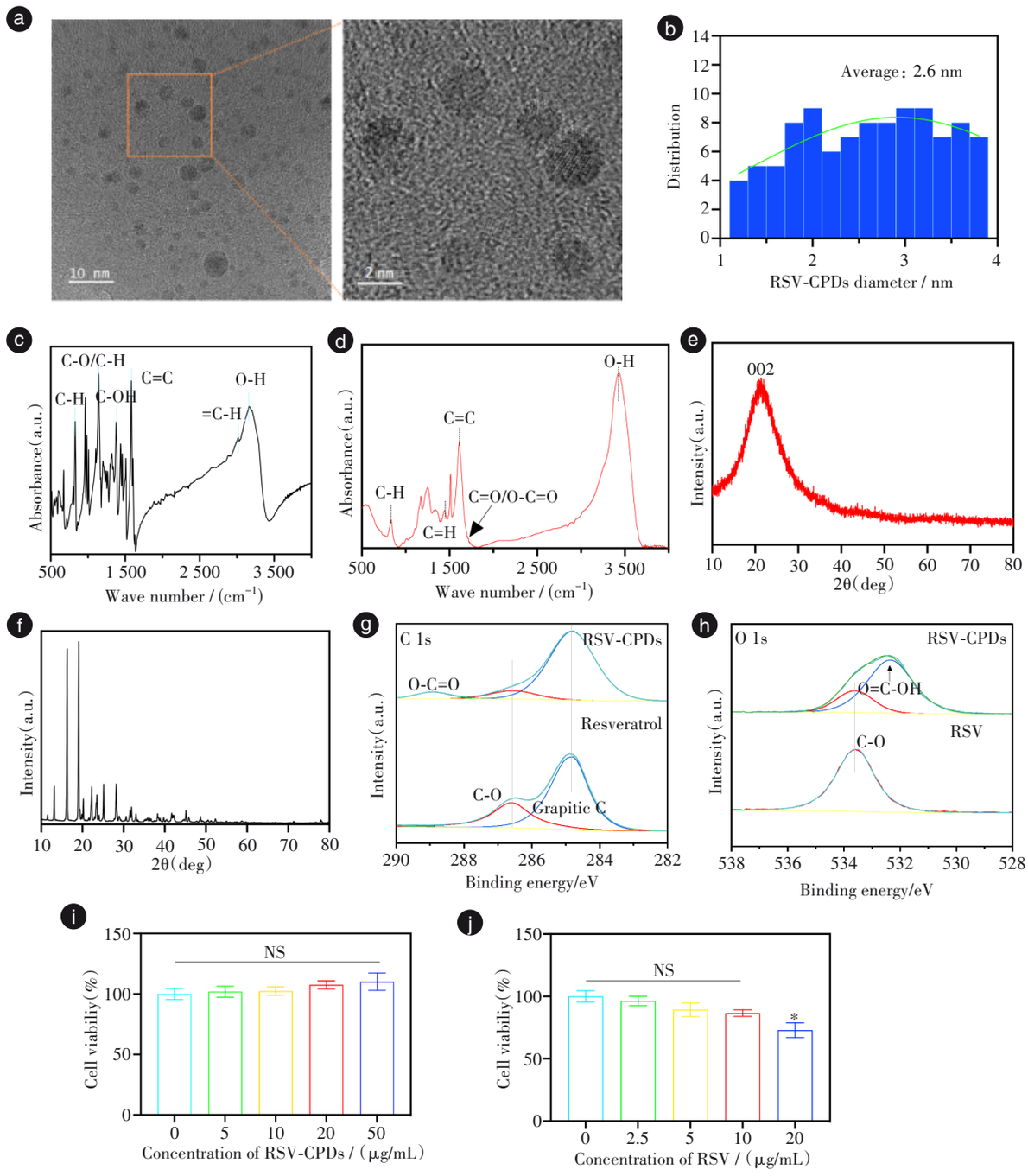

a-b: TEM images showing the size and shape of RSV-CPDs, with an average diameter of less than 3 nm; c-h: chemical characterization of RSV and RSV-CPDs. Carboxyl groups were newly formed in RSV-CPDs compared with RSV, and the structure of RSV-CPDs was amorphous, while RSV exhibited a crystalline structure; c: FTIR results of RSV; d: FTIR results of RSV-CPDs; e: XRD results of RSV-CPDs; f: XRD results of RSV; g: high-resolution C1s XPS spectra of RSV and RSV-CPDs; h: high-resolution O1s XPS spectra of RSV and RSV-CPDs. i – j: viability of RAW 264.7 cells in different treatment groups; i: viability of RAW 264.7 treated with RSV-CPDs at various concentrations (0, 5, 10, 20, 50 μg/mL); j: viability of RAW 264.7 treated with RSV at various concentrations (0, 2. 5, 5, 10, 20 μg/mL). TEM: transmission electron microscopy; FITR: Fourier transform infrared spectroscopy; XRD: X-ray diffraction; XPS: X-ray photoelectron spectroscopy; RSV: resveratrol; RSV-CPDs: resveratrol-carbonized polymer dots. *P<0.05, NS: P>0.05

Figure 1　Characterization verification and cytotoxicity test results of RSV-CPDs

图1　RSV-CPDs的表征验证及细胞毒性检测结果

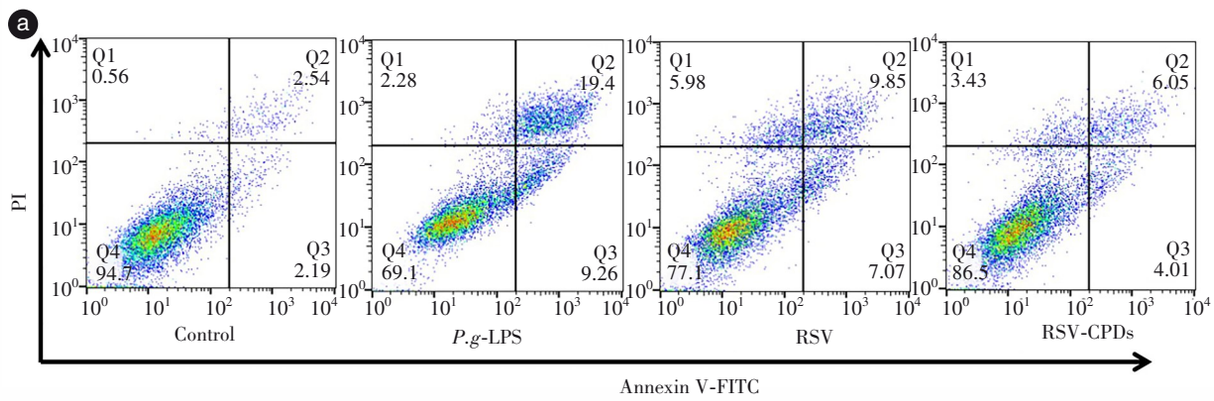

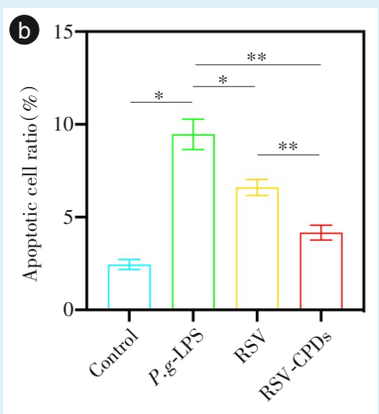

a-b: the apoptosis of RAW264.7 cells with different treatments was evaluated by flow cytometry. *P. g*-LPS successfully provoked apoptosis in RAW264.7 cells compared with the control group. Both RSV and RSV-CPDs attenuated LPS-induced apoptosis, and RSV-CPDs exerted better effects than RSV. Control group: RAW264.7 cells with no treatment; *P.g*-LPS group: RAW264.7 cells treated with *P.g*-LPS (2 μg/mL) for 24 h; RSV group: RAW264.7 cells treated with *P.g*-LPS (2 μg/mL) + RSV (10 μg/mL) for 24 h; RSV-CPDs group: RAW264.7 cells treated with *P.g*-LPS (2 μg/mL) + RSV-CPDs (50 μg/mL) for 24 h. RSV: resveratrol; RSV-CPDs: resveratrol-carbonized polymer dots. LPS: lipopolysaccharide. $^*P < 0.05$, $^{**}P < 0.01$

Figure 2　RSV-CPDs inhibited LPS-induced macrophage apoptosis

图2　RSV-CPDs抑制LPS诱导下的巨噬细胞凋亡

颜色深于RSV组。说明RSV-CPDs和RSV具有通过诱导RAW264.7向M2表型极化从而促进hPDLSCs成骨分化的能力，并且RSV-CPDs的诱导效果强于RSV。ALP定量实验结果显示：RSV-CPDs组ALP分泌显著高于对照组（P=0.006）、*P.g*-LPS+IFN-γ组（P=0.005）以及RSV组（P=0.020）。而RSV组ALP分泌情况与对照组无显著差异（P=0.146）。

接下来对上清液诱导14 d后的hPDLSCs进行ARS染色。结果显示，组间颜色趋势差异和ALP结果一致：RSV-CPDs组相对钙沉积量与对照组（P=0.006）和*P.g*-LPS+IFN-γ组（P=0.006）相比显著提升。

随后使用qRT-PCR检测不同组巨噬细胞上清液诱导的hPDLSCs成骨相关基因表达情况，结果显示，RSV-CPDs组的RUNX-2、COL-1、OCN的mRNA相较于*P.g*-LPS+IFN-γ组和对照组均有明显的上调（P<0.05），而RSV组的hPDLSCs相较于*P.g*-LPS+IFN-γ组和对照组仅在COL-1 mRNA有上调（P<0.05）。

最后使用Western blot实验进一步检测不同组巨噬细胞上清液诱导的hPDLSCs成骨相关蛋白水平，结果显示，RSV-CPDs组的RUNX-2蛋白表达均显著高于对照组（P=0.038）和*P.g*-LPS+IFN-γ组（P=0.001），而RSV组的RUNX-2蛋白水平与对照组相比无显著差异（P>0.05）。见图4。

2.5　RSV-CPDs影响炎症状态下巨噬细胞极化的机制

选用转录组学测试分析RSV-CPDs对炎症刺激下的巨噬细胞表型影响的机制。如图5a火山图所示，RSV-CPDs组与*P.g*-LPS+IFN-γ组对比，共有1 255个差异化表达基因（differentially expressed genes，DEG），包含163个下调的基因和1 092个上调的基因。GO（Gene ontology）富集分析结果显示，RSV-CPDs组与*P.g*-LPS+IFN-γ组对比，与炎症相关的干扰素-α（interferon-alpha）产生呈现下调趋势（图5b）。KEGG（Kyoto Encyclopedia of Genes and Genomes）富集分析结果证实，与*P.g*-LPS+IFN-γ组对比，RSV-CPDs组的核因子κB（nuclear factor kappa-B，NF-κB）信号通路以及肿瘤坏死因子（tumor necrosis factor，TNF）信号通路均呈现下调趋势（图5c）。

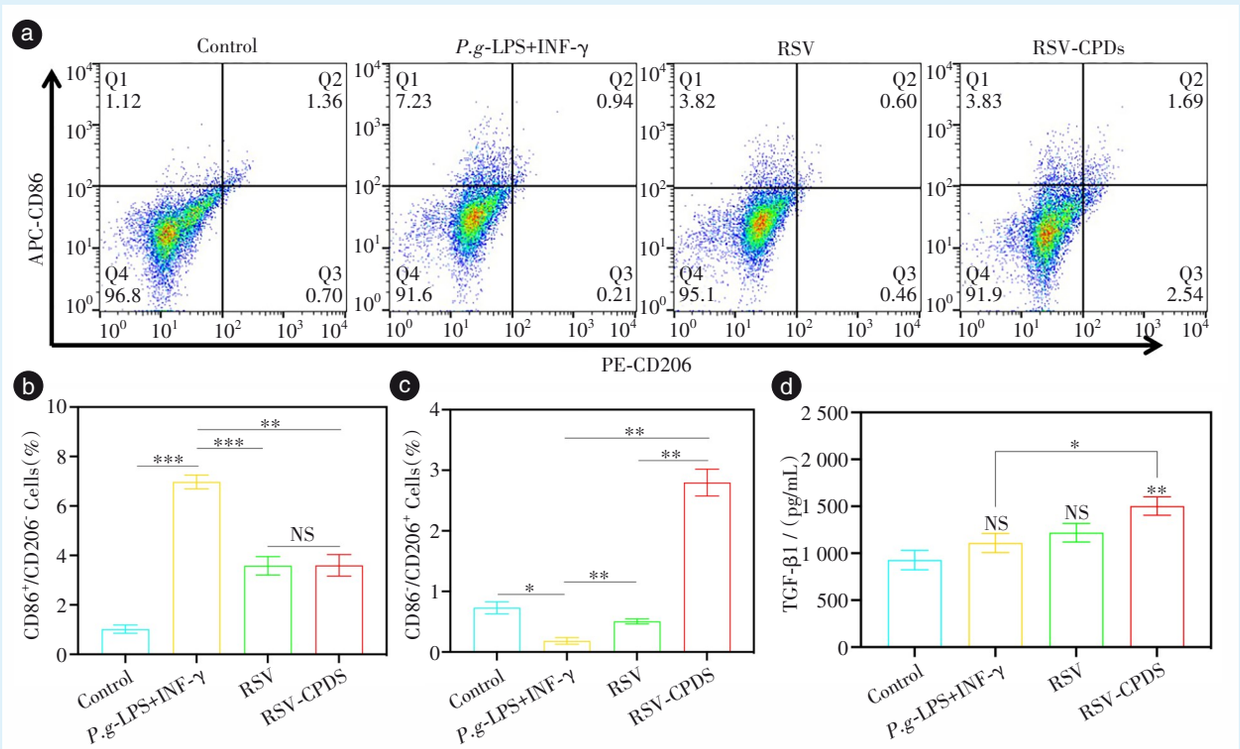

The inflammatory cell model was successfully established by *P.g*-LPS and IFN-γ treatment, as evidenced by the upregulation of CD86 (a marker of M1-phenotype macrophages), compared with the control group. Both RSV and RSV-CPDs were able to alleviate the inflammatory status, as shown by the downregulation of CD86 expression and the upregulation of CD206 (a marker of M2-phenotype macrophages). Notably, RSV-CPDs exerted better effects on promoting CD206 expression than RSV. The expression of TGF-β1 in the RSV-CPDs group was higher than that in the control and *P.g*-LPS + IFN-γ groups. a: Flow cytometry analysis of the expression of CD86 (a biomarker for M1 macrophages) and CD206 (a biomarker for M2 macrophages) in various experimental groups. The statistical analysis of $CD86^+/CD206^-$ cells (b) and $CD86^-/CD206^+$ cells (c). d: the expression of TGF-β1 in different groups detected by ELISA. Control group: RAW264.7 with no additional treatment. *P.g*-LPS+IFN-γ group: RAW264.7 treated with *P.g*-LPS (200 ng/mL) and IFN-γ (20 ng/mL) for 24 h. RSV group: RAW264.7 treated with *P.g*-LPS (200 ng/mL), IFN-γ (20 ng/mL), and RSV(10 μg/mL) for 24 h. RSV-CPDs group: RAW264.7 treated with *P.g*-LPS (200 ng/mL), IFN-γ (20 ng/mL), and RSV-CPDs (50 μg/mL) for 24 h. *P. g*-LPS: *Porphyromonas gingivalis*-lipopolysaccharide. IFN- γ: interferon-gamma. RSV: resveratrol. RSV-CPDs: resveratrol-carbonized polymer dots. ELISA: enzyme-linked immunosorbent assay. **P*<0.05, ***P*<0.01, ****P*<0.001, NS: *P*>0.05

Figure 3　RSV-CPDs promote M2 polarization of macrophages under inflammatory conditions

图3　RSV-CPDs促进炎症状态下巨噬细胞M2型极化

3　讨　论

慢性牙周炎是口腔临床常见的疾患，局部菌斑生物膜过度繁殖产生的致炎性物质会导致氧化应激以及免疫细胞功能受到抑制[18-20]。巨噬细胞作为牙周组织内免疫细胞群中的重要组成部分，其表型的变化对于牙周炎症的缓解至关重要[21]。巨噬细胞主要分为“经典型”(M1)和“替代型”(M2)，在牙周炎处于进展期时，巨噬细胞以促炎型的M1表型为主。而M2表型的巨噬细胞具有抗炎的效果，可以有效抑制炎症的进一步发展[22-23]。因此，治疗牙周炎的第一要务是控制感染、减轻炎症浸润。此外，慢性牙周炎会导致牙槽骨丧失，最终体现为牙齿松动甚至脱落。在控制炎症进展之后，逐渐减缓牙槽骨的流失则是第二要务[24-25]。综上，设计治疗慢性牙周炎的方案主要围绕着抗炎和减缓骨吸收这两个方面进行。

RSV的临床应用受制于水分散性差所导致的生物利用率低下[26-27]。本研究采用高温热解法制备的平均直径小于3 nm的RSV-CPDs则很好地弥补了这一缺陷。首先红外光谱证实了RSV-CPDs新酚羟基的形成，其次XPS数据的O1s也证实新羧酸键的出现[28]。以上结果为RSV-CPDs具有良好水分散性提供了坚实的理论支撑。此外，RSV-CPDs的生物安全性同样值得重视。其前体RSV在

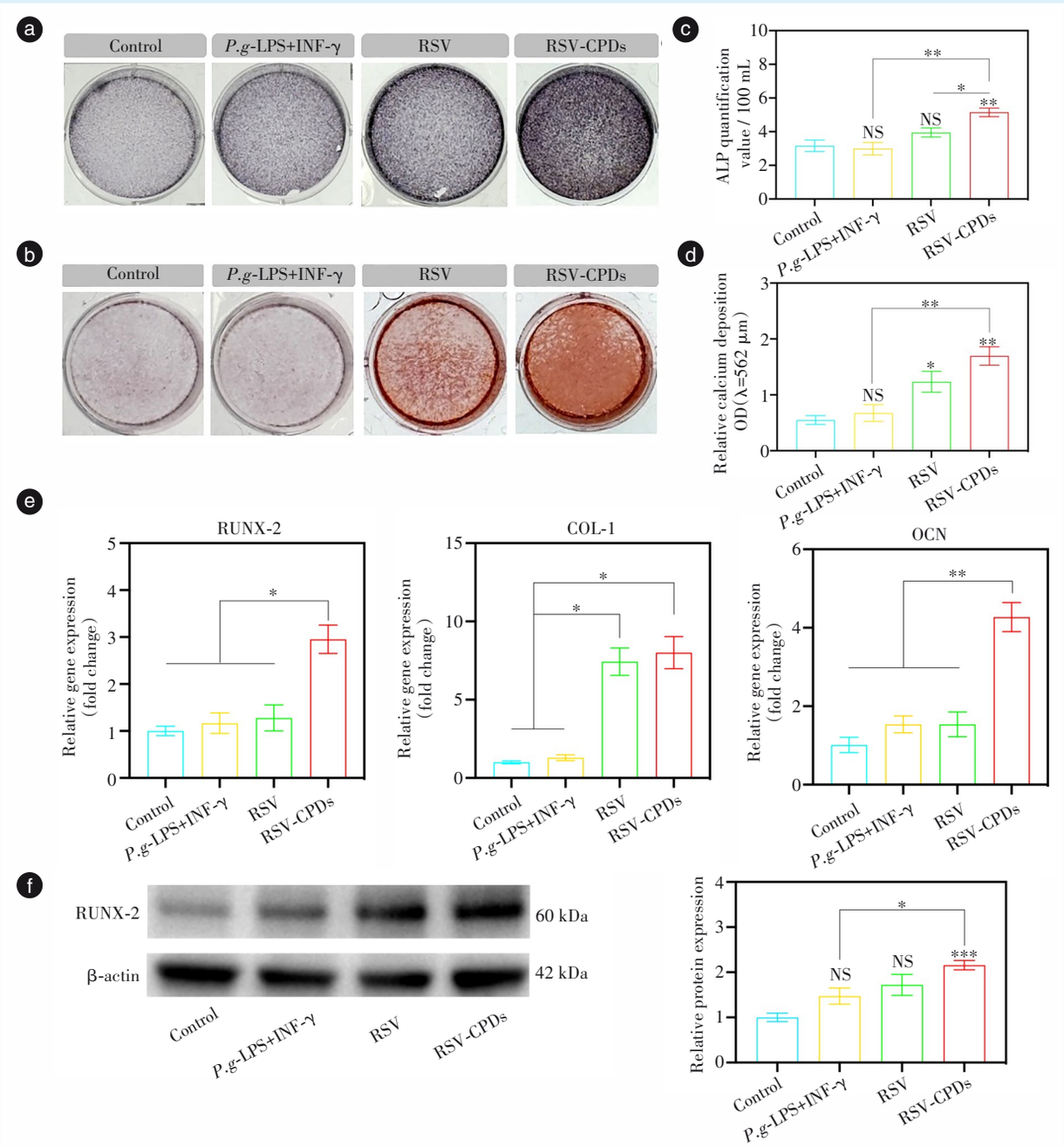

ALP activity and ARS staining were highest in the RSV-CPD group. The expression of osteogenic genes and proteins in the RSV and RSV-CPDs group was higher than in the control group and the *P.g*-LPS+IFN-γ group. Notably, the RSV-CPDs group exhibited higher expression of both osteogenic genes and proteins compared to the RSV group. Control group: the supernatant of RAW264.7 from the control group was mixed with osteogenic induction medium at a ratio of 1:1; *P.g*-LPS+IFN-γ group: the supernatant of RAW264.7 from the *P.g*-LPS+IFN-γ group was mixed with osteogenic induction medium at a ratio of 1:1; RSV group: the supernatant of RAW264.7 from the RSV group was mixed with osteogenic induction medium at a ratio of 1:1; RSV-CPDs group: the supernatant of RAW264.7 from the RSV-CPDs group was mixed with osteogenic induction medium at a ratio of 1:1; a: Alkaline phosphatase staining of hPDALSCs in various experimental groups after 7 days. b: alizarin red staining of hPDALSCs in various experimental groups after 14 days. c: ALP activity test of hPDALSCs in various experimental groups after 7 days. d: quantitative analysis of the calcium nodules in various experimental groups after 14 days. e: relative gene expression of RUNX-2, COL-1, and OCN of hPDLSCs in various experimental groups. f: protein expression of RUNX-2 of hPDLSCs in various treatments. *P. g*-LPS: *P. g*-lipopolysaccharide. IFN- γ: interferon-gamma. RSV: resveratrol. RSV-CPDs: resveratrol-carbonized polymer dots. RUNX-2: Runt-related transcription factor 2; COL-1: collagen type Ⅰ; OCN: osteocalcin; hPDLSCs: human periodontal ligament stem cells. **P*<0.05, ***P*<0.01, ****P*<0.001, NS: *P*>0.05

Figure 4　Effects of macrophage supernatants treated with different groups on osteogenic effects of periodontal ligament stem cells

图 4　不同组处理的巨噬细胞上清液对牙周膜干细胞成骨效果的影响

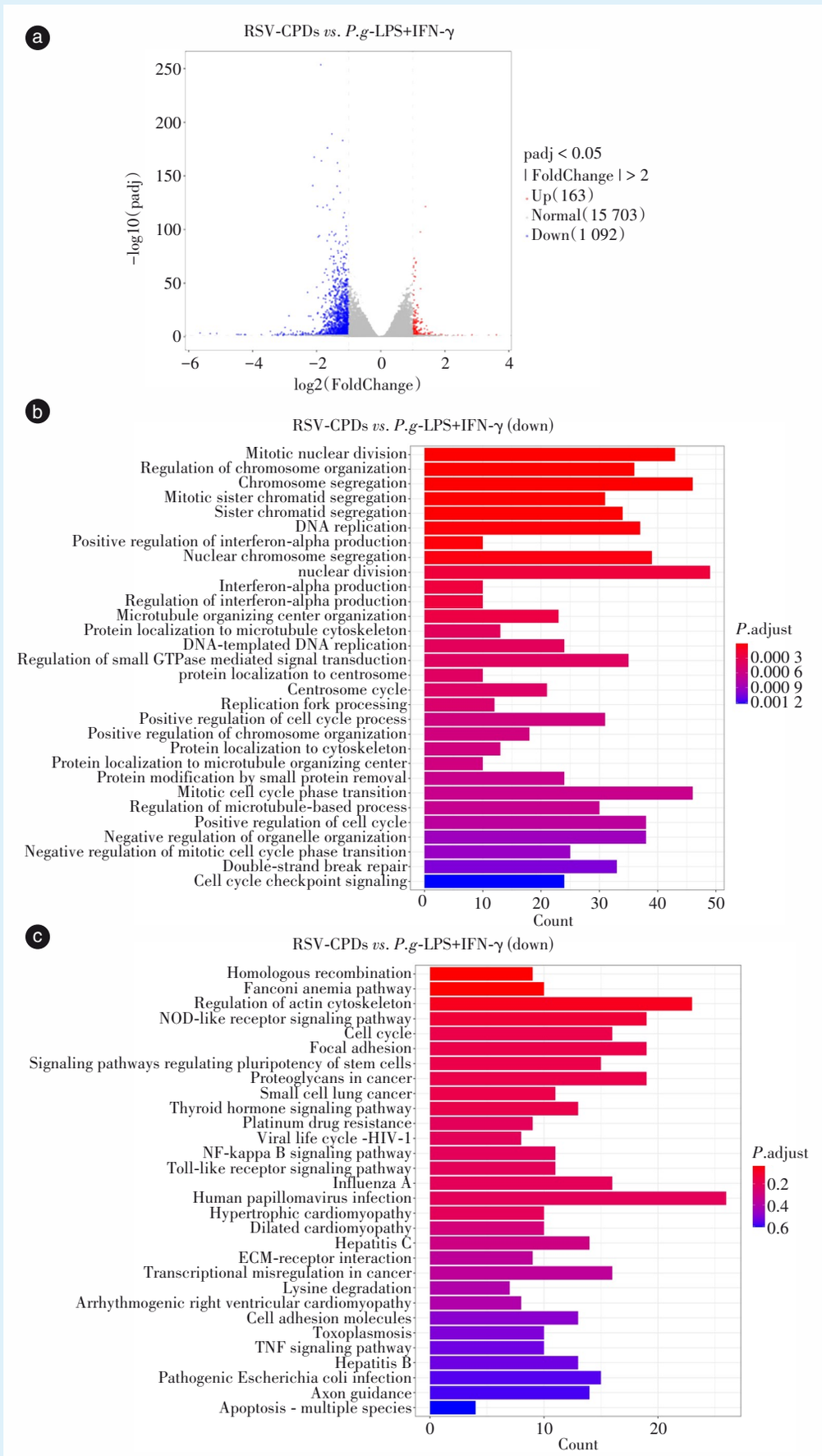

Compared with the *P. g*-LPS+IFN-γ group, RSV-CPDs effectively down-regulated inflammation-related pathways, including the NF-κB, interferon-alpha, and TNF signaling pathways. *P. g*-LPS+IFN-γ group: THP-1 cells treated with *P. g*-LPS (200 ng/mL) and IFN-γ (20 ng/mL) for 24 h. RSV-CPD group: THP-1 cells treated with *P. g*-LPS (200 ng/mL), IF-γ (20 ng/mL), and RSV-CPDs (50 μg/mL) for 24 h. a: volcano plots showing the upregulated and down-regulated genes by the RSV-CPDs treatment compared with the *P. g*-LPS+IFN-γ group ($p < 0.05$, $|\log2(FC)| \geqslant 1$). b: GO analyses of the down-regulated pathways in the RSV-CPDs group compared with the *P. g*-LPS+IFN-γ group. The red box denotes the interferon-alpha production and positive regulation of interferon-alpha production. c: KEGG analyses of the down-regulated pathways in the RSV-CPDs group compared with the *P. g*-LPS+IFN-γ group. The red box denotes the NF-κB and TNF signaling pathways

Figure 5　Transcriptome test analyzing the mechanism of the effect of RSV-CPDs on macrophage phenotype under inflammatory conditions

图5　转录组学测试分析RSV-CPDs对炎症刺激下的巨噬细胞表型影响的机制

浓度超过10 μg/mL时既对RAW264.7存在毒性，而RSV-CPDs在浓度50 μg/mL时依然保持着良好的生物安全性。因此，后续实验RSV浓度设置为10 μg/mL，RSV-CDPs浓度设置为50 μg/mL。为了体外模拟炎症微环境诱导细胞凋亡，本研究首先选用*P.g*-LPS刺激巨噬细胞[29]。在分别应用RSV和RSV-CPDs后，巨噬细胞凋亡的趋势均有一定的缓解，并且RSV-CPDs组巨噬细胞凋亡的比例低于RSV组。以上结果证明本研究制备的RSV-CPDs不仅在水溶性相较于其前体RSV有着一定程度的提升，在生物安全性方面依旧优于RSV。

炎症微环境中巨噬细胞多呈现M1表型[30-32]。选用合适的策略诱导巨噬细胞极化为M2表型对于调节炎症微环境至关重要[33]。与既往研究报道趋势一致，流式细胞术证实RSV-CPDs可以诱导RAW264.7的M1型标记物CD86显著下调[34]。此外，RSV组的巨噬细胞CD206表达与炎症刺激（*P.g*-LPS+IFN-γ）组相比有显著的统计学差异，证实其具有一定的诱导RAW264.7极化至M2表型的能力。RSV-CPDs诱导炎症刺激下的RAW264.7向M2表型极化的能力依然强于RSV，流式细胞术结果中巨噬细胞的CD206表达和RSV组存在显著差异证实了这一结论。

M2表型巨噬细胞分泌的细胞因子具有诱导干细胞成骨分化的作用[35-37]。牙周组织微环境内M2型巨噬细胞占比提升对于调节牙周膜干细胞的成骨分化功能有促进作用[38]。Ni等[39]证实金纳米粒子诱导M2表型的RAW264.7上清液可以诱导牙周膜干细胞的成骨分化。先前的实验已经证实RSV-CPDs具有良好的调节RAW264.7极化为M2表型的能力。本研究对收集到的RAW264.7上清液进行了ELISA分析，证实RSV-CPDs可以诱导巨噬细胞分泌更多量的TGF-β1。TGF-β1已经被证实具有良好地促进牙周膜干细胞成骨分化的效果[40]。然后将收集到的RAW264.7上清液与牙周膜干细胞进行共培养，依据ALP和ARS染色结果，本研究发现RSV组和RSV-CPDs组hPDLSCs分泌了更多的ALP以及钙化物，并且RSV-CPDs组效果好于RSV组。这一结果初步证实RSV-CPDs良好的间接促进骨再生效果。后续的qRT-PCR实验表明RSV-CPDs组具有更高的成骨相关基因表达，包括RUNX-2、COL-1、OCN。RUNX-2蛋白作为诱导干细胞成骨分化的“首要”转录因子[41-42]，在RSV-CPDs处理后的RAW264.7上清液培养7 d后的hPDLSCs表达量最高，上述结果进一步证实RSV-CPDs具有良好的间接促进骨再生的潜力。

为了更好地模拟RSV-CPDs应用于人体的效果，本研究选择了人源巨噬细胞-THP-1细胞进行机制研究[43]。RSV-CPDs组和*P.g*-LPS+INF-γ组相比，有很多炎症相关的信号通路呈现下调趋势，如TNF、NF-κB信号通路等。这一结果充分说明RSV-CPDs可以下调免疫细胞的炎症相关信号通路，因而诱导了巨噬细胞极化为M2表型[44-45]。

综上所述，本研究通过体外实验证实RSV-CPDs通过抑制炎症相关信号通路诱导巨噬细胞M2型极化并发挥抑制炎症的作用，M2表型巨噬细胞分泌的细胞因子可以促进hPDLSCs成骨相关基因的上调、ALP分泌的增加以及钙结节的沉积。考虑到体内微环境与体外实验存在着较大差异[46]，尤其是牙槽骨的再生是多重基因蛋白共同作用的结果，因此在后续的实验过程中将增加动物实验以及人临床相关的实验来深入探究RSV-CPDs的体内综合治疗效果以及存在的不足。

【Author contributions】 Li N performed the experiments and wrote the article. Wang YL and Liu Q analyzed the data and wrote the article. Miao LY designed the study, conceptualized and reviewed the article. All authors read and approved the final manuscript as submitted.

参考文献

[1] Hajishengallis G, Chavakis T. Local and systemic mechanisms linking periodontal disease and inflammatory comorbidities[J]. Nat Rev Immunol, 2021, 21(7): 426-440. doi: 10.1038/s41577-020-00488-6.

[2] Bartold PM. Lifestyle and periodontitis: the emergence of personalized periodontics[J]. Periodontol 2000, 2018, 78(1): 7-11. doi: 10.1111/prd.12237.

[3] Genco RJ, Van Dyke TE. Prevention: Reducing the risk of CVD in patients with periodontitis[J]. Nat Rev Cardiol, 2010, 7(9): 479-480. doi: 10.1038/nrcardio.2010.120.

[4] Pihlstrom BL, Michalowicz BS, Johnson NW. Periodontal diseases [J]. Lancet, 2005, 366(9499): 1809-1820. doi: 10.1016/S0140-6736(05)67728-8.

[5] Gunassekaran GR, Poongkavithai Vadevoo SM, Baek MC, et al. M1 macrophage exosomes engineered to foster M1 polarization and target the IL-4 receptor inhibit tumor growth by reprogramming tumor-associated macrophages into M1-like macrophages[J]. Biomaterials, 2021, 278: 121137. doi: 10.1016/j. biomaterials.2021.121137.

[6] Chen L, Yu C, Xu W, et al. Dual-targeted nanodiscs revealing the cross-talk between osteogenic differentiation of mesenchymal stem cells and macrophages[J]. ACS Nano, 2023, 17(3): 3153-3167. doi: 10.1021/acsnano.2c12440.

[7] Yan N, Xu J, Liu G, et al. Penetrating macrophage-based nanofor-

mulation for periodontitis treatment[J]. ACS Nano, 2022, 16(11): 18253-18265. doi: 10.1021/acsnano.2c05923.

[8] Cui Y, Hong S, Xia Y, et al. Melatonin engineering M2 macrophage-derived exosomes mediate endoplasmic reticulum stress and immune reprogramming for periodontitis therapy[J]. Adv Sci (Weinh), 2023, 10(27): e2302029. doi: 10.1002/advs.202302029.

[9] Nguyen DD, Luo LJ, Yang CJ, et al. Highly retina-permeating and long-acting resveratrol/metformin nanotherapeutics for enhanced treatment of macular degeneration[J]. ACS Nano, 2023, 17(1): 168-183. doi: 10.1021/acsnano.2c05824.

[10] Yao Y, Lei X, Wang Y, et al. A mitochondrial nanoguard modulates redox homeostasis and bioenergy metabolism in diabetic peripheral neuropathy[J]. ACS Nano, 2023, 17(22): 22334-22354. doi: 10.1021/acsnano.3c04462.

[11] Xia C, Zhong J, Han X, et al. The formation mechanism of carbonized polymer dots: crosslinking-induced nucleation and carbonization[J]. Angew Chem Int Ed Engl, 2024, 63(44): e202410519. doi: 10.1002/anie.202410519.

[12] Chiou YR, Lin CJ, Harroun SG, et al. Aminoglycoside-mimicking carbonized polymer dots for bacteremia treatment[J]. Nanoscale, 2022, 14(32): 11719-11730. doi: 10.1039/d2nr01959k.

[13] Li X, Kang C, Tao S, et al. A new nanomaterial-carbonized polymer dots and their applications: a review[J]. Carbon, 2025, 237: 120122. doi: 10.1016/j.carbon.2025.120122.

[14] Lu H, Liu J, Yu M, et al. Photothermal-enhanced antibacterial and antioxidant hydrogel dressings based on catechol-modified chitosan-derived carbonized polymer dots for effective treatment of wound infections[J]. Biomater Sci, 2022, 10(10): 2692-2705. doi: 10.1039/d2bm00221c.

[15] Peng H, Qiu X, Cheng M, et al. Resveratrol-loaded nanoplatform RSV@DTPF promote alveolar bone regeneration in OVX rat through remodeling bone-immune microenvironment[J]. Chem Eng J, 2023, 476: 146615. doi: 10.1016/j.cej.2023.146615.

[16] Jin SS, He DQ, Luo D, et al. A biomimetic hierarchical nanointerface orchestrates macrophage polarization and mesenchymal stem cell recruitment to promote endogenous bone regeneration[J]. ACS Nano, 2019, 13(6): 6581-6595. doi: 10.1021/acsnano.9b00489.

[17] Zhu Y, Liang H, Liu X, et al. Regulation of macrophage polarization through surface topography design to facilitate implant-to-bone osteointegration[J]. Sci Adv, 2021, 7(14): eabf6654. doi: 10.1126/sciadv.abf6654.

[18] Chen X, Huang H, Guo C, et al. Controlling alveolar bone loss by hydrogel-based mitigation of oral dysbiosis and bacteria-triggered proinflammatory immune response[J]. Adv Funct Mater, 2025, 35 (3): 2409121. doi: 10.1002/adfm.202409121.

[19] Jakubovics NS, Goodman SD, Mashburn-Warren L, et al. The dental plaque biofilm matrix[J]. Periodontol 2000, 2021, 86(1):32-56. doi: 10.1111/prd.12361.

[20] 葛叡扬, 周莹莹, 毛浩威, 等. 细胞程序性死亡在牙周炎与类风湿性关节炎关联中的桥梁作用[J]. 口腔疾病防治, 2025, 33(6): 457-465. doi: 10.12016/j.issn.2096-1456.202550030.
Ge RY, Zhou YY, Mao HW, et al. The bridging role of programmed cell death in association between periodontitis and rheumatoid arthritis[J]. J Prev Treat Stomatol Dis, 2025, 33(6): 457-465. doi: 10.12016/j.issn.2096-1456.202550030.

[21] Ge X, Hu J, Qi X, et al. An immunomodulatory hydrogel featuring antibacterial and reactive oxygen species scavenging properties for treating periodontitis in diabetes[J]. Adv Mater, 2025, 37(3): 2412240. doi: 10.1002/adma.202412240.

[22] Wei T, Pan T, Peng X, et al. Janus liposozyme for the modulation of redox and immune homeostasis in infected diabetic wounds[J]. Nat Nanotechnol, 2024, 19(8): 1178-1189. doi: 10.1038/s41565-024-01660-y.

[23] Zhou B, Magana L, Hong Z, et al. The angiocrine Rspondin3 instructs interstitial macrophage transition *via* metabolic-epigenetic reprogramming and resolves inflammatory injury[J]. Nat Immunol, 2020, 21(11): 1430-1443. doi: 10.1038/s41590-020-0764-8.

[24] Jepsen K, Sculean A, Jepsen S. Complications and treatment errors involving periodontal tissues related to orthodontic therapy[J]. Periodontol 2000, 2023, 92(1): 135-158. doi: 10.1111/prd.12484.

[25] Jepsen K, Sculean A, Jepsen S. Complications and treatment errors related to regenerative periodontal surgery[J]. Periodontol 2000, 2023, 92(1): 120-134. doi: 10.1111/prd.12504.

[26] Almeida H, Ferreira B, Fernandes-Lopes C, et al. Third-generation solid dispersion through lyophilization enhanced oral bioavailability of resveratrol[J]. ACS Pharmacol Transl Sci, 2024, 7(3): 888-898. doi: 10.1021/acsptsci.4c00029.

[27] Nakajima M, Adachi Y, Nemoto T. Computation-guided asymmetric total syntheses of resveratrol dimers[J]. Nat Commun, 2022, 13 (1): 152. doi: 10.1038/s41467-021-27546-4.

[28] Prisle NL. Surfaces of atmospheric droplet models probed with synchrotron XPS on a liquid microjet[J]. Acc Chem Res, 2024, 57 (2): 177-187. doi: 10.1021/acs.accounts.3c00201.

[29] Timblin GA, Tharp KM, Ford B, et al. Mitohormesis reprogrammes macrophage metabolism to enforce tolerance[J]. Nat Metab, 2021, 3(5): 618-635. doi: 10.1038/s42255-021-00392-w.

[30] Hu G, Su Y, Kang BH, et al. High-throughput phenotypic screen and transcriptional analysis identify new compounds and targets for macrophage reprogramming[J]. Nat Commun, 2021, 12(1): 773. doi: 10.1038/s41467-021-21066-x.

[31] Deng C, Xiao Y, Zhao X, et al. Sequential targeting chondroitin sulfate-bilirubin nanomedicine attenuates osteoarthritis *via* reprogramming lipid metabolism in M1 macrophages[J]. Adv Sci (Weinh), 2025, 12(9): e2411911. doi: 10.1002/advs.202411911.

[32] Liu T, Wang M, Liang P, et al. USP19 suppresses inflammation and promotes M2-like macrophage polarization by manipulating NLRP3 function *via* autophagy[J]. Cell Mol Immunol, 2021, 18 (10):2431-2442. doi: 10.1038/s41423-020-00567-7.

[33] Zhang J, Muri J, Fitzgerald G, et al. Endothelial lactate controls muscle regeneration from ischemia by inducing M2-like macrophage polarization[J]. Cell Metab, 2020, 31(6): 1136-1153.e7. doi: 10.1016/j.cmet.2020.05.004.

[34] Xu J, Wu M, Yang J, et al. Multimodal smart systems reprogramme macrophages and remove urate to treat gouty arthritis[J]. Nat Nanotechnol, 2024, 19(10): 1544-1557. doi: 10.1038/s41565-024-01715-0.

[35] Zhang J, Tong D, Song H, et al. Osteoimmunity-regulating biomimetically hierarchical scaffold for augmented bone regeneration[J]. Adv Mater, 2022, 34(36): e2202044. doi: 10.1002/adma.202202044.

[36] Li C, Zhang W, Nie Y, et al. Time-sequential and multi-functional 3D printed MgO_2/PLGA scaffold developed as a novel biodegradable and bioactive bone substitute for challenging postsurgical osteosarcoma treatment[J]. Adv Mater, 2024, 36(34): e2308875. doi: 10.1002/adma.202308875.

[37] Zhang F, Lv M, Wang S, et al. Ultrasound-triggered biomimetic ultrashort peptide nanofiber hydrogels promote bone regeneration by modulating macrophage and the osteogenic immune microenvironment[J]. Bioact Mater, 2023, 31: 231-246. doi: 10.1016/j.bioactmat.2023.08.008.

[38] Xiao L, Feng M, Chen C, et al. Microenvironment-regulating drug delivery nanoparticles for treating and preventing typical biofilm-induced oral diseases[J]. Adv Mater, 2023: e2304982. doi: 10.1002/adma.202304982.

[39] Ni C, Zhou J, Kong N, et al. Gold nanoparticles modulate the crosstalk between macrophages and periodontal ligament cells for periodontitis treatment[J]. Biomaterials, 2019, 206: 115-132. doi: 10.1016/j.biomaterials.2019.03.039.

[40] Manokawinchoke J, Pavasant P, Sawangmake C, et al. Intermittent compressive force promotes osteogenic differentiation in human periodontal ligament cells by regulating the transforming growth factor-β pathway[J]. Cell Death Dis, 2019, 10(10): 761. doi: 10.1038/s41419-019-1992-4.

[41] Chen J, Hu G, Li T, et al. Fusion peptide engineered "statically-versatile" titanium implant simultaneously enhancing anti-infection, vascularization and osseointegration[J]. Biomaterials, 2021, 264: 120446. doi: 10.1016/j.biomaterials.2020.120446.

[42] Komori T. Regulation of proliferation, differentiation and functions of osteoblasts by Runx2[J]. Int J Mol Sci, 2019, 20(7): 1694. doi: 10.3390/ijms20071694.

[43] Karki R, Sharma BR, Tuladhar S, et al. Synergism of TNF-α and IFN-γ triggers inflammatory cell death, tissue damage, and mortality in SARS-CoV-2 infection and cytokine shock syndromes[J]. Cell, 2021, 184(1): 149-168.e17. doi: 10.1016/j.cell.2020.11.025.

[44] Xie H, Huang X, Li B, et al. Biomimetic nanoplatform for targeted rheumatoid arthritis therapy: modulating macrophage niches through self-sustaining positive feedback-driven drug release mechanisms[J]. Adv Sci (Weinh), 2025, 12(15): e2416265. doi: 10.1002/advs.202416265.

[45] 刘森庆, 张华, 陈艳艳, 等. 白藜芦醇通过抑制MAPKs/NF-κB信号通路治疗小鼠种植体周围炎[J]. 口腔疾病防治, 2024, 32(11): 845-852. doi: 10.12016/j.issn.2096-1456.202440228.
Liu SQ, Zhang H, Chen YY, et al. Resveratrol treats peri-implantitis in mice *via* inhibiting the MAPKs/NF-κB signaling pathway[J]. J Prev Treat Stomatol Dis, 2024, 32(11): 845-852. doi: 10.12016/j.issn.2096-1456.202440228.

[46] Urzì O, Gasparro R, Costanzo E, et al. Three-dimensional cell cultures: the bridge between *in vitro* and *in vivo* models[J]. Int J Mol Sci, 2023, 24(15): 12046. doi: 10.3390/ijms241512046.

（编辑　周春华）

官网